IEEE Access
Multidisciplinary ⋮ Rapid Review ⋮ Open Access Journal

Received 25 March 2024, accepted 7 April 2024, date of publication 19 April 2024, date of current version 1 May 2024.

Digital Object Identifier 10.1109/ACCESS.2024.3391306

RESEARCH ARTICLE

Path Clustering for Radio Propagation Prediction With Moving Object in Indoor Environment

MASAYUKI SHIRAKAWA[1], REI FURUKAWA[1], GILBERT CHING[1], (Member, IEEE), KENSHI HORIHATA[1], (Member, IEEE), YUKIKO KISHIKI[1], (Member, IEEE), HIROKAZU SAWADA[2], (Member, IEEE), AZRIL HANIZ[2], (Member, IEEE), TAKESHI MATSUMURA[2], (Member, IEEE), HOMARE MURAKAMI[2], (Member, IEEE), AND FUMIHIDE KOJIMA[2], (Member, IEEE)

[1]Kozo Keikaku Engineering Inc., Nakano-ku, Tokyo 164-0012, Japan
[2]National Institute of Information and Communications Technology, Wireless Networks Research Center, Yokosuka, Kanagawa 239-0847, Japan

Corresponding author: Masayuki Shirakawa (masayuki-shirakawa@kke.co.jp)

This work was supported in part by the Ministry of Internal Affairs and Communications through the Research and Development for the Realization of High-Precision Radio Wave Emulator in Cyberspace under Grant JPJ000254, and in part by YAZAKI Corporation.

ABSTRACT To simulate radio propagation in a dynamic indoor environment such as a factory operating with moving people and automated guided vehicles (AGV), we devised a technique to determine shielding losses by moving objects based on ray tracing. For a moving object environment, conventional ray-tracing methods require simulation of each snapshot of a moving object. This conventional technique requires too much time for real-time predictions. The proposed method first calculates the static environment using the ray-tracing method without the moving object, and then the shielding loss caused by a moving object is included through post-processing. To enhance efficiency, 3D path clustering was employed, which significantly reduced the total number of paths and computation time. For comparison, we measured the radio-propagation environment of an existing Japanese factory. The root-mean-square errors (RMSEs) and correlation coefficients of the proposed and conventional methods were compared based on the experimental results, wherein the indicators of the proposed method were comparable to those of the conventional method even though the number of paths was reduced. Furthermore, the proposed method reduces the computation time to approximately 5% of that of the conventional method.

INDEX TERMS Ray tracing, clustering methods, indoor environment, radiowave propagation.

I. INTRODUCTION

For 5G and 6G, various applications have been explored using wireless communications between numerous devices. This could lead to a shortage of the spectrum and a serious decline in spectrum efficiency. For efficient and rapid implementation of a new system in an existing environment, it is appropriate to evaluate the wireless environment with the help of emulation [1], [2]. We conducted research on radio-propagation models of a new wireless emulation system [3]. The ray tracing method is a widely used technique for predicting indoor and outdoor propagation environments and various frequency bands [4], [5], [6], [7], [8], [9]. However, because of the long computation time required for ray-tracing calculations, more efficient computation is required to predict propagation environments considering moving objects, as repeated simulations are necessary [10], [11], [12], [13].

Some studies introduced methods for extracting data from a preprocessed database for ray-tracing acceleration [14], [15], [16]. 3GPP Technical Report Release 14 is a hybrid channel model that combines a stochastic model with a ray tracing model [17]. Hybrid models have been proposed in various studies to reduce computation

The associate editor coordinating the review of this manuscript and approving it for publication was Giovanni Angiulli.

times [18], [19], [20], [21]. The GPU acceleration technique contributes to reducing the computational cost of ray-tracing [22], [23], [24], [25]. Some studies have attempted to kinetically reflect the motion of objects on ray-traced paths [10], [26]. Recently, there have been reports on the application of machine learning and artificial intelligence in the prediction of mobile radio propagation [27], [28], [29], [30], [31]. Notably, studies have been conducted on quantum algorithms for radio propagation [32].

In this study, we present a technique for simulating a dynamic propagation environment involving mobile objects. Our approach incorporates the impact of moving objects based on the outcomes obtained through a ray tracing methodology designed for a static propagation environment. To reduce computational cost, we created a method for clustering ray-traced paths with similar 3D routes. We further calculated the path loss and delay spread for clustered ray-traced paths. The concept of this approach was introduced in a previous study [33].

In this letter, we describe the details of our approach, which were not mentioned in the previous letter owing to space limitations. Subsequently, we present experimental results conducted in a factory in operation and ray-tracing results using the proposed method and the conventional method, referred to as the sequential ray-tracing method [10].

To utilize the proposed method, it is necessary to determine two parameters, which are discussed in a later section. These parameters were optimized to minimize the root-mean-square error (RMSE) between the calculated and experimental results. In the previous letter [33], we determined the parameters for RMSE, which were derived from the proposed and conventional methods. In this study, we compared the simulation performance of these methods based on the experimental results. Our findings demonstrate that the proposed method's shielding loss is more accurate to the experimental results compared to the conventional method. Furthermore, the computation time of the proposed method was considerably shorter than that of the conventional method.

In the following sections, we present the details of the proposed method and the experiments conducted in an indoor factory environment. Subsequently, we present and compare the proposed method with the conventional method based on experimental results.

II. PROPOSED METHOD

The conventional method of simulating a radio-propagation environment with mobile objects requires performing ray-trace calculations sequentially, using multiple 3D models that place moving objects at varying locations. However, owing to its long computation time, the ray-tracing method is not efficient in predicting dynamic radio propagation in real time. In our proposed method, we first simulated radio propagation in a static indoor environment in advance, thereby improving efficiency. We then computed the impact of mobile objects, such as the human body and an automated guided vehicle (AGV), on radio propagation. Fig. 1 shows the flowchart of the proposed method. This section presents the specifications of the proposed method.

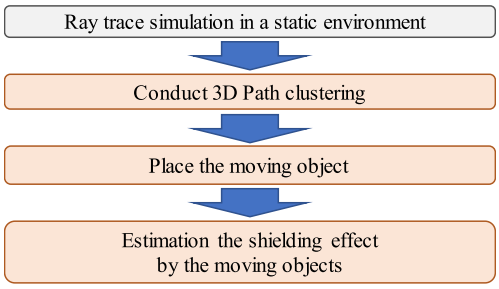

FIGURE 1. The flowchart of the proposed method.

We analyzed their interactions with ray-traced paths to compute the impact of moving objects. However, as both the number of mobile objects and ray-traced paths increased, the computation time of this approach also increased. We introduce the concept of trajectory clustering to minimize the number of paths and computation time [34], [35]. This involves defining parameters, such as the trajectory of clustered paths, their width, and the received power of the clustered paths. The impact of the moving objects was calculated based on these parameters.

A. 3D PATH CLUSTERING

In the field of radio propagation, the distance between paths is typically determined using multipath components, including arrival angle, departure angle, and delay time [36], [37]. However, in such cases, this method may not properly estimate the impact of moving objects, because these parameters do not account for the intermediate trajectory of ray-traced paths. To address this issue, we used the discrete Frechet distance [38] to estimate the similarity between ray-traced paths and cluster them (see Fig. 2). To calculate the discrete Frechet distance, we measured the distance between interaction points on ray-traced paths based on the Euclidean metric.

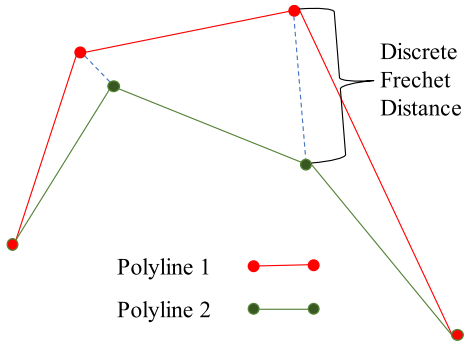

FIGURE 2. Description of the discrete frechet distance.

During calculation the discrete Frechet distance, pairs of points can move on two polylines without going backwards. The discrete Frechet distance measures the shortest distance sufficient to traverse two polylines, as shown in Figure 2.

Fig. 3 shows a schematic of the proposed 3D path-clustering algorithm.

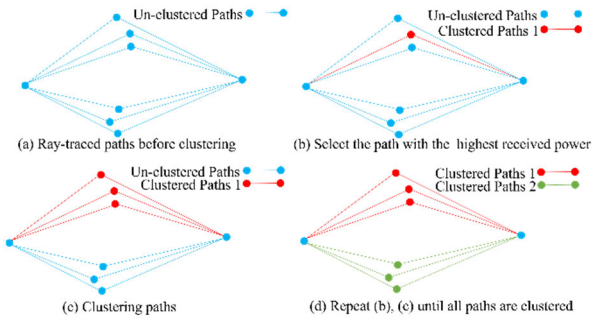

FIGURE 3. Description of 3D path clustering.

A clustering threshold value was used to cluster the ray-traced paths (Fig. 3 (a)). The paths are classified as part of the same cluster if the Frechet distance from the path with the highest received power is below this threshold (Fig. 3 (b) and (c)). This process was repeated until all paths were clustered (Fig. 3 d).

B. PARAMETERS OF CLUSTERED PATHS

To estimate the shielding effect on the clustered paths determined in the previous section, we established various parameters for the clustered paths, as illustrated in Fig. 4.

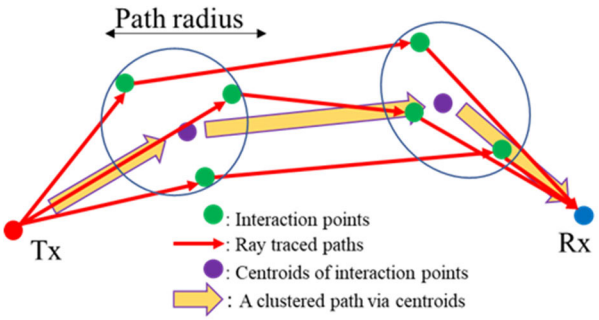

FIGURE 4. The concept of a path cluster's route.

The route of the clustered paths is determined by the path with the highest received power among clustered paths. Interaction points without Tx and Rx were allocated to the nearest interaction point of the highest-power path, although the number of interaction points on each path was different. The route of the clustered path is determined by the centroids of the allocated interaction points and is weighted by the received power of the ray-traced path to which each interaction point belongs. Hence, the number of points on the route of the clustered path is the same as the number of interaction points on the highest-power path. The width of the route of the clustered path is determined by the variances, and weighted by the received power of the ray-traced path to which each interaction point belongs. The total received power is determined by the complex summation of the received powers of the clustered paths.

C. PATH LOSS ON CLUSTERED PATHS

To calculate the path loss on clustered paths, we considered moving objects such as the human body and AGV as screens. The screen size of the human body and AGV defined refer to the 3D models used in our ray-trace simulation. Screen size is described in the next section. We estimated the shielding effect on the received power of a path for each segment of clustered paths. Fig. 5 (a)–(c) show the flowchart of the shielding effect estimation.

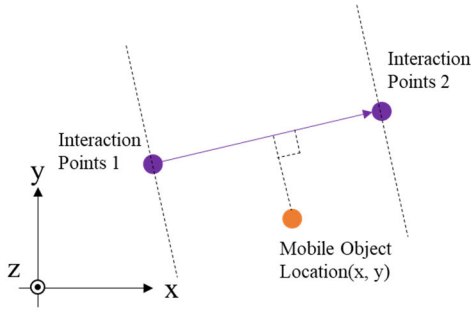

(a) Check whether the mobile object is in an area between interaction points

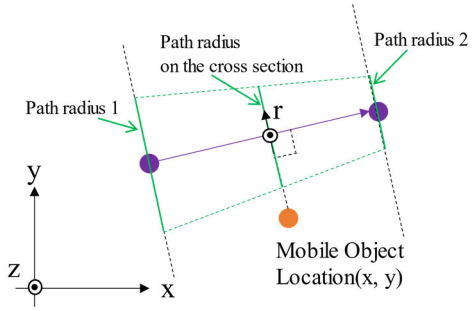

(b) Identify the plane for calculation of the shielding loss.

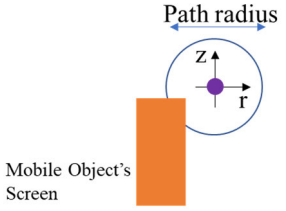

(c) Estimate the shielding effect

FIGURE 5. The flowchart of shielding effect estimation.

The shielding effect of the i-th segment C_i, is calculated when the intersection of a straight line along that segment and a perpendicular line from the center of the moving object fell within the segment. This calculation is performed on the cross-section perpendicular to the x-y plane, where the center of the moving object is located. C_i was determined using

Eq. (2), as follows:

$$S = \min\left\{\sum_i C_i, 1\right\} \tag{1}$$

$$C_i = \frac{1}{2\pi\ (\varepsilon r_i)^2} \iint_A \exp\left(-\frac{r^2+z^2}{2\ (\varepsilon r_i)^2}\right) \mathrm{drdz} \tag{2}$$

where x and y represent the axes on the cross-section and r_i denotes the path width that is linearly interpolated along the i-th segment of the route. A is the area occupied by the moving object's screen and ε is the width coefficient used to tune the shielding loss. C_i indicates the proportion of overlap between the screen and clustered paths. The shielding effect S in Equation (1) represents the addition of C_i from all segments in a clustered path route.

III. EXPERIMENT AND SIMULATION CONDITIONS

We compared the proposed method with the conventional method based on the measurement results of the radio propagation environment in an active manufacturing field in an existing factory owned by the YAZAKI Corporation. The following section describes the measurement campaign conducted in the factory and the ray-tracing simulation conditions for the conventional and proposed methods.

A. EXPERIMENTAL CONDITIONS IN AN INDOOR FACTORY IN OPERATION

The experimental setup is shown in Fig. 6. Table 1 lists the transmitter and receiver configurations used in these experiments.

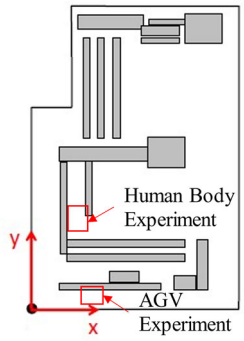

(a) Overview of indoor factory and experiment areas

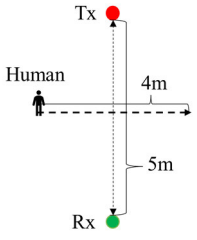

(b) Human body experiment

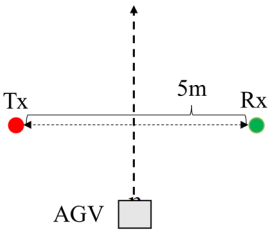

(c) AGV experiment

FIGURE 6. Schematic diagram of experiment in the active manufacturing field.

TABLE 1. The transmitter and receiver settings.

Items	Setting 1	Setting 2
Scenarios	Human Body Experiment	Human Body Experiment, AGV Experiment
Frequency [GHz]	5.25	28.35
Transmitter Power [dBm]	20.59	18.98
Antenna patterns of Transmitter and Receiver	Isotropic	Isotropic
Total Cable Loss [dB]	4.84	14.4

The transmitter and receiver were placed 5 m apart. For the human-body shielding experiment (Fig. 5(b)), the antenna height was 1.4 m, and for the AGV shielding experiment (Fig. 5(c)), it was 1.5 m. In the human-body shielding experiment, the person stood between the transmitter and receiver and moved every 20 cm, and an obstruction occurred in the line-of-sight (LOS) when the person moved 2 m. The received power was averaged over a period of 30 seconds for each location where the participant stood.

During the AGV shielding experiment, the transmitter and receiver were placed at the site of AGV operation, obstructing the LOS. The AGV was moving at a speed of 0.75 m/s within the factory. The AGV-shielding experiment was conducted at 28 GHz band. The experimental data were aligned according to the time slots to match and average the peaks of shielding loss for each slot.

B. SIMULATION CONDITIONS

A 3D factory model was created for the ray-tracing simulation using the factory drawings. Fig. 7 shows the exterior and interior of the factory 3D model. Owing to confidentiality, the manufacturing line equipment was modeled as rectangular solids, as shown in Fig. 7.

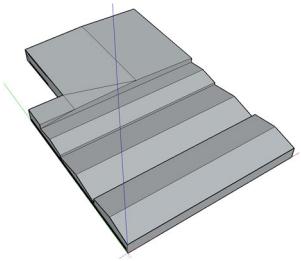

(a) Exterior of Factory 3D model

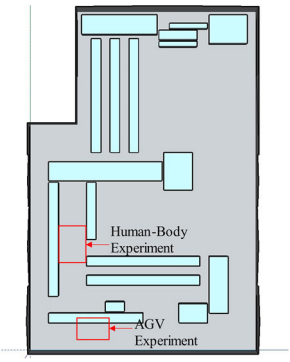

(b) Interior of Factory 3D model

FIGURE 7. 3D model of the active manufacturing field.

For the moving object, we created a 3D model of the human body and AGV, as shown in Fig. 7. The human body model

was an octagonal prism measuring 1.7 m height and 0.3 m width. The AGV model is a rectangular solid that measures 1.67 m in height, 1.44 m in length, and 1.128 m in width, as indicated in the AGV drawing.

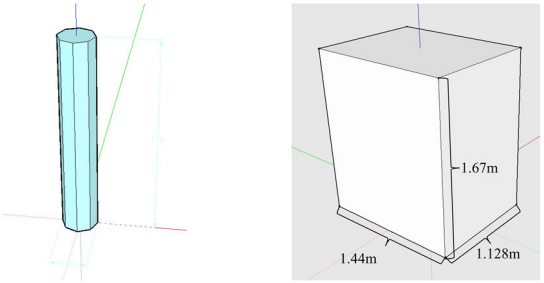

(a) The Human Body Model (b) The AGV Model

FIGURE 8. The human body model and AGV model.

As mentioned in the previous section, we defined the screen size from the 3D model of the human body and AGV. The human body screen measures 1.7 m in height and 0.3 m in width [39], while the AGV measures 1.67 m in height and 1.284 m in width, as per the drawing of the AGV used in the factory where the experiment was conducted. The width of the AGV screen was derived from the average value of the length and width of the AGV 3D model (Fig. 8 (b)).

Table 2 presents the parameters used in the ray tracing simulations. Wireless InSite [40] software was used to perform ray-tracing simulations.

TABLE 2. Raytracing conditions.

Items	Settings
Transmission Frequency	5.25 GHz, 28.35004 GHz
Max Reflection Number	3
Max Transmission Number	1
Max Diffraction Number	2
Raytracing Method	Ray Launching
Ray Spacing	0.1 degree

To determine the radio propagation parameters, several materials were applied to both 3D factory models and 3D models of moving objects. Factory walls, floors, and ceilings are made of concrete, windows are made of glass, and manufacturing lines consist of metals. The electrical parameters for both concrete and glass were calculated based on the transmission frequency, as per ITU-R Recommendation P.2040-1 [41] (Table 3). The human body is assumed to consist of a saline solution with a concentration of 9 ppt, whereas AGV is assumed to be composed of metals. The electrical parameters of the saline solution were calculated based on the transmission frequency, as per ITU-R recommendation P.527-6 [42]. The metallic material is assumed to be a perfect conductor.

Experiments on the human body and AGV shielding were conducted in separate areas of the factory, both of which are indicated in Fig. 6 (b) by the red squares. The calculations were based on the coordinates of the transmitter/receiver, and the experiment was performed, as shown in Table 4.

TABLE 3. Material properties for raytracing simulation.

Material	Frequency [GHz]	Relative Permittivity	Conductivity [S/m]
Concrete	5.25	5.31	0.1248
Concrete	28.35	5.31	0.4887
Glass	5.25	6.27	0.0311
Glass	28.35	6.27	0.2321
Saline Water	5.25	72.006	7.119
Saline Water	28.35	25.845	53.32

TABLE 4. Locations of transmitters and receivers.

Experiments	Items	Coordinates (X[m], Y[m], Z[m])
Human Body	Transmitter	(18.87, 56.35, 1.4)
	Receiver	(18.87, 51.35, 1.4)
AGV	Transmitter	(26.636, 14.798, 1.5)
	Receiver	(31.636, 14.798, 1.5)

To conduct a human body shielding simulation using the conventional method, we prepared 21 models, each with a different location of the human body model in accordance with the conditions of the human body shielding experiment. Subsequently, calculations were performed for each model. For the AGV shielding simulation using the conventional method, we prepared 48 models, each with a different location of the AGV model at 25 cm steps along the route of AGV operation. The average received power at each of the three points was compared to the measured results.

IV. COMPARISON BETWEEN PROPOSED METHOD AND SEQUENTIAL RAY TRACING

In this section, we compare the proposed method with the conventional method. We first present the path loss and delay spread results of both the experiment and simulation and then move on to the computation time.

A. COMPARISON IN PATH LOSS

We present both experimental and simulation results obtained using the proposed and conventional methods with path loss. To employ the proposed method, the clustering threshold and width coefficient were tuned to minimize the RMSE between the measured and computed results for each experiment (Fig. 9).

For each result presented in Fig. 9, the RMSEs relative to the measured results were minimized using the parameters (red points in Fig. 9) provided in Table 5. When different parameters resulted in the same RMSE value, a smaller clustering threshold or width coefficient was used. The parameters listed in Table 5 were used for 3D path clustering and estimation of the shielding effect of the proposed method.

The results for human body shielding are presented in Fig. 10. The experimental results showed that the path loss

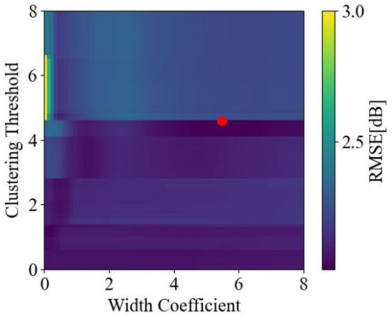

(a) Human Body, 5 GHz band

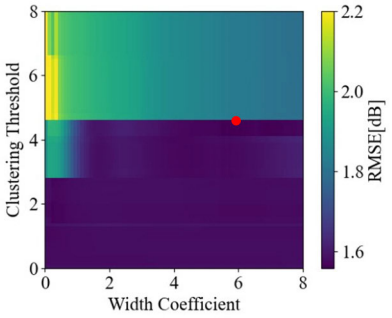

(b) Human body, 28 GHz band

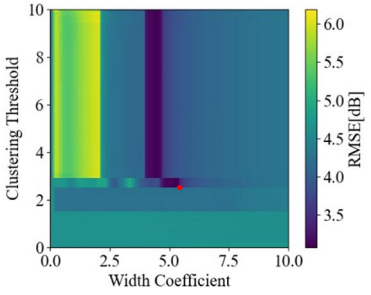

(c) AGV, 28GHz band

FIGURE 9. RMSE color map for clustering parameters.

TABLE 5. Clustering parameters.

Object	Frequency [GHz]	Clustering Threshold	Width Coefficient (ε)
Human Body	5.25	4.6	5.5
Human Body	28.35	4.6	5.8
AGV	28.35	2.7	5.4

increased by approximately 5 dB when the LOS path was obstructed by the human body at both the frequencies. For the results at 5 GHz band (Fig. 10 (a)), a similar trend was observed in the results of the proposed method. However, the results of the proposed method were smaller than the experimental results when the LOS path was not obstructed by the human body. The manufacturing lines in the factory were modeled as rectangular solids (Fig. 7). Therefore, the path reflected by the manufacturing line might have been overestimated at 5 GHz band. For the conventional method, the path loss fluctuates significantly owing to the passing of

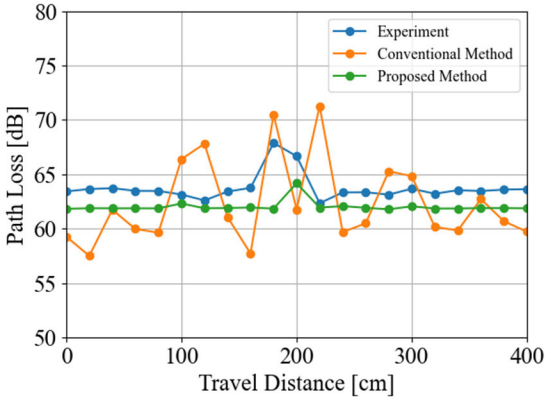

(a) Results at 5 GHz band

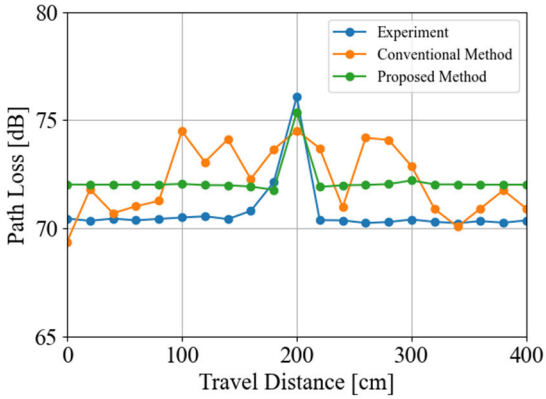

(b) Results at 28 GHz band

FIGURE 10. Path loss by human body passing through LOS.

the human body compared with the other results. Furthermore, in the results at 5 GHz band and 200 cm, the path loss was significantly smaller than that of the experiment and proposed method. The diffraction paths from the human body compensate for the reduction in the received power owing to LOS obstruction in the results of the conventional method. At 28 GHz band, the results of the proposed method were larger than the experimental results, where the human body did not obstruct the LOS path. This tendency is completely different from the results obtained at 5 GHz. The scattering paths from the surroundings, such as the manufacturing lines, are underestimated in the proposed method because of the roughly modeled manufacturing lines. In the results of the conventional method at 28 GHz band, a high fluctuation appeared, similar to that at 5 GHz band. Hence, the conventional method tends to overestimate the paths from the human body.

Table 6 presents the RMSEs and correlation coefficients obtained from the experimental results for each method.

The RMSEs for each method are sufficiently small for ray-trace simulation because a prediction error within a few decibels is acceptable [43]. Both indicators demonstrate that the proposed method is superior to conventional methods. For the conventional method, the highly fluctuating path loss caused an increase in the RMSE and a weak correlation

TABLE 6. Comparison indicator against experiment results.

Indicator	Frequency [GHz]	Conventional Method	Proposed Method
RMSE [dB]	5.25	4.09	2.01
	28.35	2.16	1.56
Correlation coefficient	5.25	0.16	0.50
	28.35	0.39	0.92

with. However, for the proposed method, the RMSE and correlation coefficient at 28 GHz band are better than those at 5 GHz band. This result suggests that the proposed method is effective at high frequencies.

Fig. 11 displays the results of the AGV shielding at 28 GHz band. The horizontal axis was converted to the travel distance using an AGV speed of 0.75 m/s. The path loss peak in the experimental results is plotted at a travel distance of 200 cm.

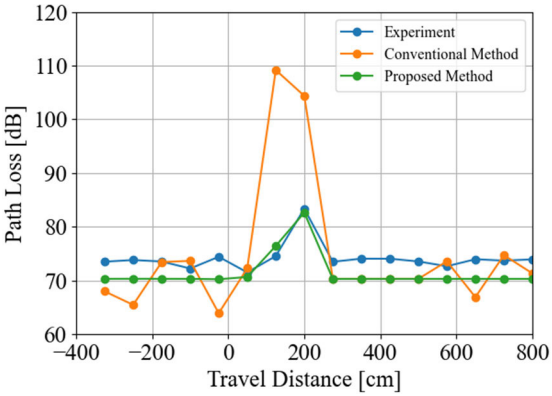

FIGURE 11. Path loss by AGV at 28 GHz band.

The proposed method yielded better results in terms of RMSE and correlation coefficient than the conventional method. The path-loss peak calculated using the conventional method varied from approximately 20 to 30 dB compared with the experimental results. In this case, the ray-traced path is diffracted 2 times in the AGV 3D model. Generally, ray-trace simulations based on the Geometrical Theory of Diffraction have difficulty in calculating the multiple diffraction loss; [44] therefore, multiple diffraction on the AGV could cause an extremely high path loss against the measurement results.

In conclusion, the proposed method provides more accurate results than the conventional method for path-loss estimation.

B. COMPARISON IN DELAY SPREAD

In this section, we present the simulation and experimental results for delay spread and compare them. The clustering parameters for the proposed method are the same as those described in the previous section.

The delay spread change by human body shielding is shown in Fig. 12.

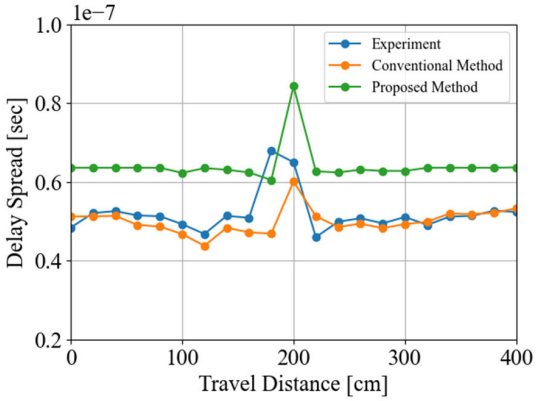

(a) Results at 5 GHz band

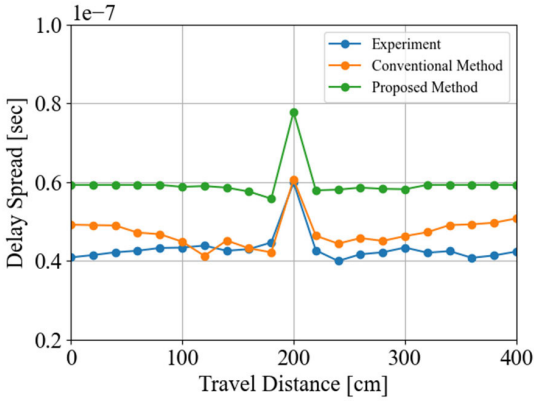

(b) Results at 28 GHz band

FIGURE 12. Delay spread by human body passing through LOS.

For all results in Fig. 12, the delay spread increases at 200 cm when the human body obstructs the LOS path. The results of the proposed method are larger than those of the experimental and conventional methods for almost all the travel distances. The proposed method does not consider paths that interact with obstructions such as the human body. In this study, a human body was placed near the LOS path. Therefore, the delay spreads of the conventional method and experiment were smaller than those of the proposed method. For the results at 28 GHz band, the delay spread of the conventional method became larger than that of the experiment from 0 cm to 100 cm and from 300 cm to 400 cm in travel distance. In general, propagation loss increases at higher frequencies. This can result in a smaller received power of the paths from the human body and a larger delay spread in an area far from the LOS path.

The RMSE and correlation coefficient from the experiment results are shown in Table 7.

The conventional method performed better than the proposed method in terms of the RMSE values. This is because the delay spread of the proposed method is shifted from the experimental results, which do not consider the paths from the obstructions. However, the correlation coefficients of both the methods are weak. For the results at 5 GHz band, the delay spread of the experimental results became significantly

TABLE 7. Comparison indicator against experiment results.

Indicator	Conventional Method	Proposed Method
RMSE [dB]	11.08	3.08
Correlation coefficient	0.63	0.89

TABLE 8. Comparison indicator against experiment results.

Indicator	Frequency [GHz]	Conventional Method	Proposed Method
RMSE [sec]	5.25	5.18e-9	1.58e-8
	28.35	5.24e-9	1.65e-8
Correlation coefficient	5.25	0.38	0.49
	28.35	0.64	0.92

larger than those of both methods at 180 cm. This caused the correlation coefficient to become weaker than that of the proposed method, and suggests that both methods failed to estimate the effect of the human body placed by the side of the LOS path. For the results at 28 GHz band, the differences between the experiment and conventional method increased in the area far from the LOS path, as mentioned above. This caused the proposed method to have a smaller correlation coefficient than that of the proposed method.

Fig. 13 shows the delay spread of AGV shielding at 28 GHz band. The horizontal axis is shown in Fig. 11.

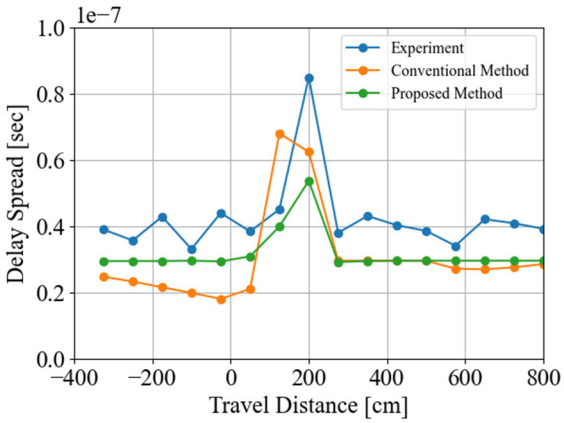

FIGURE 13. Delay spread by AGV at 28 GHz band.

For all the results, the delay spread becomes larger when the AGV in operation obstructs the LOS path. However, the delay spread of the proposed method was smaller than that in the experiment, and the proposed method before the AGV obstructed the LOS path. The delay spread of the conventional method at 125 cm was higher than that of the experiment and proposed method. The AGV is roughly modeled as a rectangle, similar to the manufacturing line. This likely caused an overestimation of the paths from the AGV and an obstruction by the AGV. Furthermore, the AGV 3D model overlapped with the manufacturing line after the AGV passed the LOS path. This causes the difference between the conventional method and the proposed method to become smaller than other travel distances.

The RMSE and correlation coefficient from the experiment results are shown in Table 9.

TABLE 9. Comparison indicator against experiment results.

Indicator	Conventional Method	Proposed Method
RMSE [sec]	1.58e-8	1.24e-8
Correlation coefficient	0.67	0.92

For both indicators, the proposed method performed better than the conventional one. As mentioned above, the roughness of the 3D models likely caused higher fluctuations in the results of the conventional method. However, the details of the 3D model and the computation time of ray tracing simulations exhibit a trade-off relationship.

In conclusion, the proposed method is better than the conventional method, except for the RMSE for human-body obstruction. However, the correlation coefficient at 5GHz band was weak, even for the proposed methods. This indicates that the proposed method is more effective at 28 GHz band than at 5 GHz band.

C. COMPARISON IN COMPUTATION TIME

The computation times of the proposed and conventional methods were compared through simulation of human body experiments within a factory. Python version 3.11 was used to post-process the proposed method for creating clustered paths and calculating the effects of the moving object. The machine specifications for the ray-tracing calculations are listed in Table 7.

TABLE 10. Machine specifications.

Items	Settings
Processor	AMD Ryzen 9 3950X 16-Core Processor 3.49 GHz
RAM	64 GB
GPU	NVIDIA GeForce RTX 2070 SUPER
OS	Windows 10 Pro
System	64-bit operating system, x64 base processor

The path losses of the proposed and conventional methods were calculated 21 times for each location of the human body model under the experimental conditions in the factory. In addition, a static propagation environment simulation was conducted as a pre-calculation step for the proposed method. The average computation times at 5 GHz band and 28 GHz band were compared between the proposed and conventional methods, as listed in Table 8.

The proposed method significantly reduces the total computation time required to simulate the experiment in a factory. Compared to the conventional method, it achieves

TABLE 11. Computation time.

Items	Proposed Method[s]	Conventional Method[s]
Pre-Computation Time	1011.53	--
Computation Time for Simulating the Human Body Shielding	0.90	20202.03
Total Computation Time	1012.43	20202.03

a 20x reduction. Moreover, the average total computation time for simulating the human body shielding was only 0.90 seconds compared to the conventional method's 20,202.03 seconds. Except for the case in which the indoor factory layout changes, the precomputation step of the proposed method requires no recalculation. Thus, if the parameters of the proposed method can be reused, it will be more efficient than the conventional method in calculating the dynamic propagation environment.

V. CONCLUSION

In this paper, we present a more efficient method for calculating dynamic propagation environments, specifically within a factory in operation, using the ray-tracing method. The proposed method pre-computes the static propagation environment through ray tracing, and then post-processes the effects of moving objects. We used the three-dimensional Fréchet distance between paths to cluster the ray-tracing paths during post-processing.

The RMSEs and correlation coefficients of the experimental results for the path loss of the human body and AGV were compared between the proposed and conventional methods. Consequently, the RMSEs and correlation coefficients of the proposed method were better than those of the conventional method, except for the RMSE of human body obstruction, even though the proposed method reduced the number of paths. In particular, at 28 GHz band, the proposed method yielded better results in terms of the correlation coefficient than the conventional method. However, ignoring the paths from the human body and AGV causes a difference between the results of the experiment and the proposed method. Therefore, to improve the proposed method, we have to consider the paths from the human body and AGV. With respect to computation time, the proposed method is approximately 20 times faster than the conventional method. These results demonstrate the superiority of the proposed method over the conventional method for simulating a dynamic propagation environment.

REFERENCES

[1] T. Matsumura, H. Sawada, T. Miyachi, F. Kojima, H. Harai, A. Sakaguchi, Y. Nishigori, and H. Harada, "Development and initial implementation of large-scale wireless emulator toward beyond 5G," in *Proc. 25th Int. Symp. Wireless Pers. Multimedia Commun. (WPMC)*, Herning, Denmark, Oct. 2022, pp. 199–204.

[2] F. Kojima, T. Miyachi, T. Matsumura, H. Sawada, H. Harai, and H. Harada, "A large-scale wireless emulation environment with interaction between physical and virtual radio nodes for beyond 5G systems," in *Proc. IEEE 33rd Annu. Int. Symp. Pers., Indoor Mobile Radio Commun. (PIMRC)*, Kyoto, Jpn, Sep. 2022, pp. 1–6.

[3] Y. Kishiki, G. S. Ching, W. Okamura, S. Iwasaki, R. Furukawa, K. Sugiyama, S. Wu, M. Shirakawa, and M. Kawamura, "On the radio propagation modeling for advanced radio emulation system based on cyber physical fusion," *IEICE Transacitons Commun. (Jpn. Ed.)*, vol. J105-B, no. 11, pp. 862–871, 2022.

[4] S. Y. Seidel and T. S. Rappaport, "Site-specific propagation prediction for wireless in-building personal communication system design," *IEEE Trans. Veh. Technol.*, vol. 43, no. 4, pp. 879–891, Nov. 1994.

[5] G. Liang and H. L. Bertoni, "A new approach to 3-D ray tracing for propagation prediction in cities," *IEEE Trans. Antennas Propag.*, vol. 46, no. 6, pp. 853–863, 1998.

[6] J. Zhang, J. Lin, P. Tang, W. Fan, Z. Yuan, X. Liu, H. Xu, Y. Lyu, and L. Tian, "Deterministic ray tracing: A promising approach to THz channel modeling in 6G deployment scenarios," *IEEE Commun. Mag.*, vol. 62, no. 2, pp. 48–54, 2024.

[7] H. B. Eldeeb, M. Uysal, S. M. Mana, P. Hellwig, J. Hilt, and V. Jungnickel, "Channel modelling for light communications: Validation of ray tracing by measurements," in *Proc. 12th Int. Symp. Commun. Syst., Netw. Digit. Signal Process. (CSNDSP)*, Jul. 2020, pp. 1–6.

[8] F. Aghaei, H. B. Eldeeb, L. Bariah, S. Muhaidat, and M. Uysal, "Comparative characterization of indoor VLC and MMW communications via ray tracing simulations," *IEEE Access*, vol. 11, pp. 90345–90357, 2023.

[9] F. Aghaei, H. B. Eldeeb, and M. Uysal, "A comparative evaluation of propagation characteristics of vehicular VLC and MMW channels," *IEEE Trans. Veh. Technol.*, vol. 73, no. 1, pp. 4–13, Jan. 2024.

[10] D. Bilidashi, E. M. Vitucci, and V. Degli-Esposti, "On dynamic ray tracing and anticipative channel prediction for dynamic environments," *IEEE Trans. Antennas Propag.*, vol. 71, no. 6, pp. 5335–5348, 2023.

[11] N. Zhang, J. Dou, L. Tian, X. Yuan, X. Yang, S. Mei, and H. Wang, "Dynamic channel modeling for an indoor scenario at 23.5 GHz," *IEEE Access*, vol. 3, pp. 2950–2958, 2015.

[12] F. Fuschini, E. M. Vitucci, M. Barbiroli, G. Falciasecca, and V. Degli-Esposti, "Ray tracing propagation modeling for future small-cell and indoor applications: A review of current techniques," *Radio Sci.*, vol. 50, no. 6, pp. 469–485, Jun. 2015.

[13] S. Y. Lim, Q. P. Soo, A. Adam, D. W. G. Lim, Z. Yun, and M. F. Iskander, "Towards a comprehensive ray-tracing modeling of an urban city with open-trench drains for mobile communications," *IEEE Access*, vol. 5, pp. 2300–2307, 2017.

[14] A. Toscano, F. Bilotti, and L. Vegni, "Fast ray-tracing technique for electromagnetic field prediction in mobile communications," *IEEE Trans. Magn.*, vol. 39, no. 3, pp. 1238–1241, May 2003.

[15] S. Hussain and C. Brennan, "An efficient ray validation technique for ray-tracing in urban microcellular environments," *IEEE Antennas Wireless Propag. Lett.*, vol. 22, no. 6, pp. 1401–1405, Jun. 2023.

[16] T. Kim Geok, F. Hossain, S. Kamal Abdul Rahim, O. Elijah, A. A. Eteng, C. Theng Loh, L. Li Li, C. P. Tso, T. Abd Rahman, and M. Nour Hindia, "3D RT adaptive path sensing Method: RSSI modelling validation at 4.5 GHz, 28 GHz, and 38 GHz," *Alexandria Eng. J.*, vol. 61, no. 12, pp. 11041–11061, 2022.

[17] "Technical specification group radio access network: Study on channel model for frequencies from 0.5 to 100 GHz," 3rd Gener. Partnership Project (3GPP), Version 17.0.0, Tech. Rep. (TR) 38.901, Mar. 2022.

[18] P. Große, C. Schneider, G. Sommerkorn, and R. Thomä, "A hybrid channel model based on WINNER for vehicle-to-X application," 2016, *arXiv:1601.05929*.

[19] S. Priebe and T. Kurner, "Stochastic modeling of THz indoor radio channels," *IEEE Trans. Wireless Commun.*, vol. 12, no. 9, pp. 4445–4455, Sep. 2013.

[20] Y. Chen, Y. Li, C. Han, Z. Yu, and G. Wang, "Channel measurement and ray-tracing-statistical hybrid modeling for low-terahertz indoor communications," *IEEE Trans. Wireless Commun.*, vol. 20, no. 12, pp. 8163–8176, Dec. 2021.

[21] S. Arikawa and Y. Karasawa, "A simplified MIMO channel characteristics evaluation scheme based on ray tracing and its application to indoor radio systems," *IEEE Antennas Wireless Propag. Lett.*, vol. 13, pp. 1737–1740, 2014.

[22] Y. Tao, H. Lin, and H. Bao, "GPU-based shooting and bouncing ray method for fast RCS prediction," *IEEE Trans. Antennas Propag.*, vol. 58, no. 2, pp. 494–502, Feb. 2010.

[23] J. Tan, Z. Su, and Y. Long, "A full 3-D GPU-based beam-tracing method for complex indoor environments propagation modeling," *IEEE Trans. Antennas Propag.*, vol. 63, no. 6, pp. 2705–2718, Jun. 2015.
[24] A. N. Cadavid, D. G. Ibarra, and S. L. Salcedo, "Using 3-D video game technology in channel modeling," *IEEE Access*, vol. 2, pp. 1652–1659, 2014.
[25] C. Pyo, H. Sawada, and T. Matsumura, "A deep learning-based indoor radio estimation method driven by 2.4 GHz ray-tracing data," *IEEE Access*, vol. 11, pp. 138215–138228, 2023.
[26] X. Zhang, N. Sood, J. K. Siu, and C. D. Sarris, "A hybrid ray-tracing/vector parabolic equation method for propagation modeling in train communication channels," *IEEE Trans. Antennas Propag.*, vol. 64, no. 5, pp. 1840–1849, May 2016.
[27] Y. Zhang, J. Sun, G. Gui, H. Gacanin, and H. Sari, "A generalized channel dataset generator for 5G new radio systems based on ray-tracing," *IEEE Wireless Commun. Lett.*, vol. 10, no. 11, pp. 2402–2406, Nov. 2021.
[28] M. Hirose, T. Imai, S. Wu, S. Iwasaki, G. S. Ching, and Y. Kishiki, "Ray tracing parameter optimization system in mobile radio propagation prediction," in *Proc. IEEE 33rd Annu. Int. Symp. Pers., Indoor Mobile Radio Commun. (PIMRC)*, Kyoto, Japan, Sep. 2022, pp. 01–05.
[29] M. Hirose, T. Imai, S. Wu, S. Iwasaki, G. S. Ching, and Y. Kishiki, "A ray tracing parameter optimization system in mobile radio propagation prediction," in *Proc. Int. Workshop Antenna Technol. (iWAT)*, Dublin, Ireland, May 2022, pp. 269–270.
[30] L. Azpilicueta, M. Rawat, K. Rawat, F. M. Ghannouchi, and F. Falcone, "A ray launching-neural network approach for radio wave propagation analysis in complex indoor environments," *IEEE Trans. Antennas Propag.*, vol. 62, no. 5, pp. 2777–2786, May 2014.
[31] D. He, K. Guan, D. Yan, H. Yi, Z. Zhang, X. Wang, Z. Zhong, and N. Zorba, "Physics and AI-based digital twin of multi-spectrum propagation characteristics for communication and sensing in 6G and beyond," *IEEE J. Sel. Areas Commun.*, vol. 41, no. 11, pp. 3461–3473, Nov. 2023.
[32] R. Novak, "Quantum algorithms in electromagnetic propagation modelling for telecommunications," *IEEE Access*, vol. 11, pp. 111545–111565, 2023.
[33] M. Shirakawa, R. Furukawa, G. Ching, Y. Kishiki, H. Sawada, T. Matsumura, and F. Kojima, "Path clustering and calculation of shielding effect for dynamic indoor environment simulation," *IEICE Commun. Exp.*, vol. 11, no. 9, pp. 596–600, 2022.
[34] J.-G. Lee, J. Han, and K.-Y. Whang, "Trajectory clustering: A partition-and-group framework," in *Proc. ACM SIGMOD Int. Conf. Manage. Data, Beijing, China, Assoc. Comput. Machinery*, 2007, pp. 593–604.
[35] J.-G. Lee, J. Han, and X. Li, "A unifying framework of mining trajectory patterns of various temporal tightness," *IEEE Trans. Knowl. Data Eng.*, vol. 27, no. 6, pp. 1478–1490, Jun. 2015.
[36] X. Wu, C.-X. Wang, J. Sun, J. Huang, R. Feng, Y. Yang, and X. Ge, "60-GHz millimeter-wave channel measurements and modeling for indoor office environments," *IEEE Trans. Antennas Propag.*, vol. 65, no. 4, pp. 1912–1924, Apr. 2017.
[37] C.-C. Chong and S. K. Yong, "A generic statistical-based UWB channel model for high-rise apartments," *IEEE Trans. Antennas Propag.*, vol. 53, no. 8, pp. 2389–2399, Aug. 2005.
[38] T. Eiter and H. Mannila. (1994). *Computing Discrete Frechet Distance*. [Online]. Available: http://www.kr.tuwien.ac.at/staff/eiter/et-archive/cdtr9464.pdf
[39] ITU. (2021). *Guidelines for Evaluation of Radio Interface Technologies for IMT-2020*. Accessed: Sep. 15, 2023. [Online]. Available: https://www.itu.int/pub/R-REP-M.2412-2017
[40] Remcom. *Wireless InSite 3D Wireless Prediction Software*. [Online]. Available: https://www.remcom.com/wireless-insite-em-propagation-software
[41] ITU. (Jul. 2015). *Effects of Building Materials and Structures on Radiowave Propagation Above About 100 MHz*. Accessed: Sep. 15, 2023. [Online]. Available: https://www.itu.int/rec/R-REC-P.2040/en
[42] ITU. *Electrical Characteristics of the Surface of the Earth*. Accessed: Sep. 15, 2023. [Online]. Available: https://www.itu.int/rec/R-REC-P.527/en
[43] V. Erceg, S. J. Fortune, J. Ling, A. J. Rustako, and R. A. Valenzuela, "Comparisons of a computer-based propagation prediction tool with experimental data collected in urban microcellular environments," *IEEE J. Sel. Areas Commun.*, vol. 15, no. 4, pp. 677–684, May 1997.
[44] B. Yang, L. Xu, N. Qiu, J. Yang, and G. Wang, "Simulation of multiple acoustic diffraction based on an iterative ray tracing method," in *Proc. J. Phys., Conf.*, vol. 2450, 2023, Art. no. 012001.

MASAYUKI SHIRAKAWA received the Ph.D. degree from the Department of Physics, Graduate School of Science, Tokyo University of Science, in 2020. In 2020, he joined Kozo Keikaku Engineering Inc.. Since then, he has been engaged in system development. His research interests includes radio wave propagation.

REI FURUKAWA received the master's degree in mechanical engineering from the Graduate Program, Seikei University, in 2007, and the Ph.D. degree in advanced program from Tokyo University of Marine Science and Technology, in 2020. In 2007, he joined Kozo Keikaku Engineering Inc., where he resumed his work, in 2014. From 2011 to 2014, he was engaged in research on cognitive radio with the Advanced Telecommunications Research Institute International (ATR). His focus is on actively engaging in system development. His research interest includes radio-wave propagation.

GILBERT CHING (Member, IEEE) was born in Manila, Philippines, in 1974. He received the B.S. and M.S. degrees in electrical engineering from the University of the Philippines, in 1996 and 2003, respectively, and the D.E. degree from Tokyo Institute of Technology, Tokyo, Japan, in 2007. From 1996 to 2003, he was an Instructor with the University of the Philippines. Since 2007, he has been with Kozo Keikaku Engineering Inc. His research interests include radio wave propagation measurements, simulations, and analyses. He is a member of the IEICE. He received one of the Best Student Paper Awards from PIMRC '06 and ITS 07.

KENSHI HORIHATA (Member, IEEE) received the B.S. degree from Tokyo Institute of Technology, Tokyo, Japan, in 2003. He joined Panasonic Mobile Communications Company Ltd., as an Antenna and Propagation Engineer for mobile communication systems. From 2012 to 2015, he was engaged in research on cognitive radio with the Advanced Telecommunication Research Institute International (ATR), assigned by Panasonic. In 2021, he joined Kozo Keikaku Engineering Inc. His current interests include simulation analyses related to radio wave propagation, antennas, and radio wave phenomena.

YUKIKO KISHIKI (Member, IEEE) received the B.S. and M.S. degrees in electronics engineering from The University of Electro-Communications, Tokyo, Japan, in 2001 and 2003, respectively, and the D.E. degree from Tokyo Institute of Technology, Tokyo, in 2010.

In 2003, she joined Kozo Keikaku Engineering Inc., Japan. She has been engaged in radio-propagation research and development of a ray-tracing simulator. Her current research interests include wireless propagation, ray tracing, and geometric optics. She is a member of the IEICE. She was a recipient of the Student Paper Award presented by the International Symposium on Antenna and Propagation, in 2008.

HIROKAZU SAWADA (Member, IEEE) received the B.E., M.E., and Ph.D. degrees in electrical and electronic engineering from Gifu University, Japan, in 1997, 1999, and 2002, respectively. From 2002 to 2005, he was a Researcher with Tohoku Institute of Technology, Japan. From 2005 to 2007, he was an Expert Researcher with the National Institute of Information and Communications Technology (NICT), Japan. From 2007 to 2009, he was a Lecturer with Tohoku Institute of Technology. From 2009 to 2013, he was an Assistant Professor with the Research Institute of Electrical Communications (RIEC), Tohoku University, Japan. Since 2013, he has been a Researcher and the Research Manager with NICT.

AZRIL HANIZ (Member, IEEE) received the B.E. degree from the Department of Electrical and Electronic Engineering, Tokyo Institute of Technology (Tokyo Tech), Tokyo, Japan, in 2010, and the M.Eng. and Dr.Eng. degrees from the Department of International Development Engineering, Tokyo Tech, in 2012 and 2016, respectively. From 2016 to 2019, he was a specially appointed Lecturer with Tokyo Tech. Since April 2019, he has been a Researcher with the National Institute of Information and Communications Technology, Tokyo. His research interests include localization, cognitive radio, sensor networks, and signal processing.

TAKESHI MATSUMURA (Member, IEEE) received the M.S. degree in electronic engineering and the Ph.D. degree in nano-mechanics engineering from Tohoku University, Sendai, Japan, in 1998 and 2010, respectively.

From 1998 to 2007, he was engaged in the research and development of wireless communications devices in some companies. In April 2007, he joined the National Institute of Information and Communications Technology (NICT), Tokyo, Japan, as a Researcher with the Smart Wireless Laboratory and engaged in the white-space communication systems and 5th generation mobile communication systems. From April 2016 to March 2019, he was an Associate Professor with the Graduate School of Informatics, Kyoto University, Kyoto, Japan. He is currently the Director of the Wireless Systems Laboratory, NICT, and a Researcher with the Graduate School of Informatics, Kyoto University. His research interests include white-space communication systems, wide-area wireless network systems, 5G mobile communication systems, and wireless emulation technologies.

HOMARE MURAKAMI (Member, IEEE) received the B.E. and M.E. degrees in electronic engineering from Hokkaido University, in 1997 and 1999, respectively. Since 1999, he has been with the Communications Research Laboratory, Ministry of Post and Telecommunications. From 2003 to 2005, he was a Visiting Researcher with Aalborg University. He is currently reorganized with the National Institute of Information and Communications Technology (NICT), where he is a Senior Researcher with the Wireless Systems Laboratory, the Wireless Networks Research Center, and the Network Research Institute. His research interests include spectrum sharing, cognitive radio networking, the private use of 5G/B5G, networking for robotics, and IP mobility. He is a member of the IEICE.

FUMIHIDE KOJIMA (Member, IEEE) received the B.E., M.E., and D.E. degrees in electrical communications engineering from Osaka University, Osaka, Japan, in 1996, 1997, and 1999, respectively. In 1999, he joined the Communications Research Laboratory, Ministry of Posts and Telecommunications, where he has been engaged in research on ITS, disaster radio, and wireless grids, including SUN and smart grids. He is currently the Director General of the ICT Testbed Research and Development Promotion Center, Social Innovation Unit, Open Innovation Promotion Headquarters, and National Institute of Information and Communications Technology (NICT), Tokyo, Japan. His current interests include research, development, standardization, and promotion of B5G radio communication technology, including the IoT radio communication technology and B5G testbed construction and management.